ADVANCED MATERIALS
www.advmat.de

Unusual Two-Step Assembly of a Minimalistic Dipeptide-Based Functional Hypergelator

Priyadarshi Chakraborty, Yiming Tang, Tomoya Yamamoto, Yifei Yao, Tom Guterman, Shai Zilberzwige-Tal, Nofar Adadi, Wei Ji, Tal Dvir, Ayyalusamy Ramamoorthy, Guanghong Wei, and Ehud Gazit**

Self-assembled peptide hydrogels represent the realization of peptide nanotechnology into biomedical products. There is a continuous quest to identify the simplest building blocks and optimize their critical gelation concentration (CGC). Herein, a minimalistic, de novo dipeptide, Fmoc-Lys(Fmoc)-Asp, as an hydrogelator with the lowest CGC ever reported, almost fourfold lower as compared to that of a large hexadecapeptide previously described, is reported. The dipeptide self-assembles through an unusual and unprecedented two-step process as elucidated by solid-state NMR and molecular dynamics simulation. The hydrogel is cytocompatible and supports 2D/3D cell growth. Conductive composite gels composed of Fmoc-Lys(Fmoc)-Asp and a conductive polymer exhibit excellent DNA binding. Fmoc-Lys(Fmoc)-Asp exhibits the lowest CGC and highest mechanical properties when compared to a library of dipeptide analogues, thus validating the uniqueness of the molecular design which confers useful properties for various potential applications.

Dr. P. Chakraborty, T. Guterman, S. Zilberzwige-Tal, Dr. W. Ji, Prof. T. Dvir, Prof. E. Gazit
School of Molecular Cell Biology and Biotechnology
George S. Wise Faculty of Life Sciences
Tel Aviv University
Tel Aviv 6997801, Israel
E-mail: ehudg@post.tau.ac.il

Y. Tang, Y. Yao, Prof. G. Wei
Department of Physics
State Key Laboratory of Surface Physics
Key Laboratory for Computational Physical Sciences (MOE)
Multiscale Research Institute of Complex Systems, and Collaborative Innovation Center of Advanced Microstructures (Nanjing)
Fudan University
Shanghai 200433, P. R. China
E-mail: ghwei@fudan.edu.cn

Dr. T. Yamamoto, Prof. A. Ramamoorthy
Biophysics and Department of Chemistry
Biomedical Engineering
Macromolecular Science and Engineering
University of Michigan
Ann Arbor, MI 48109, USA

N. Adadi, Prof. T. Dvir, Prof. E. Gazit
Department of Materials Science and Engineering
Iby and Aladar Fleischman Faculty of Engineering
Tel Aviv University
Tel Aviv 6997801, Israel

The ORCID identification number(s) for the author(s) of this article can be found under https://doi.org/10.1002/adma.201906043.

DOI: 10.1002/adma.201906043

Self-assembly is the spontaneous free-energy-driven association of building blocks into organized structures.[1] Ubiquitous in the natural world, molecular self-assembly is of paramount importance for the evolution, progress, and amelioration of life.[2] The range of implications of molecular self-assembly are diverse, from fabrication of self-assembling devices[3–5] to deciphering the self-assembly of misfolded proteins into stable fibers associated with human disease.[6–8] Peptides, as fragments of proteins, resemble the structural and functional characteristics of this major class of biomolecules. Over the last two decades, the self-assembly of peptides has attracted immense research interest due to their intrinsic biocompatibility, biodegradability, relatively small size, and interesting physical properties. These features led to the application of self-assembling peptides in biology as well as nanotechnology.[9–16]

Hydrogels are one typical outcome of the self-assembly process, where the formed fibers entangle to generate a 3D network.[17,18] Due to their potent hydrogelation, peptides have been extensively studied as supramolecular hydrogelators for various potential biotechnological and biomedical applications.[16,19–23] Peptide-based hydrogels have even been translated from academic research to commercial applications. A prime example is Corning PuraMatrix, a protected synthetic 16-mer peptide containing arginine-alanine-aspartate repeats. PuraMatrix self-assembles into fibers that resemble the extracellular matrix[24] and has been applied in tissue regeneration.[25] While various peptide hydrogelators have been utilized for biomedical applications, peptides of low critical gelation concentration (CGC) are especially desirable due to the low wt% required for obtaining a hydrogel. Such peptides should not only be more cost-effective, but could also present increased biocompatibility in cases where the monomeric hydrogelator is somewhat cytotoxic. Additionally, these hydrogels would also be effective in blood coagulation and wound healing applications due to their excellent hydrogelation propensity. Owing to their unidirectional H-bonding and π-stacking interactions,[18] some peptide hydrogelators (either modified or unmodified) exhibit a very low CGC value. The lowest CGC till date, 0.007 wt%, was reported for the hexadecapeptide hydrogelator FEFEFKFKFEFEFKFK.[26] Another hydrogelator, NapGFFY-NMe, exhibited a CGC value

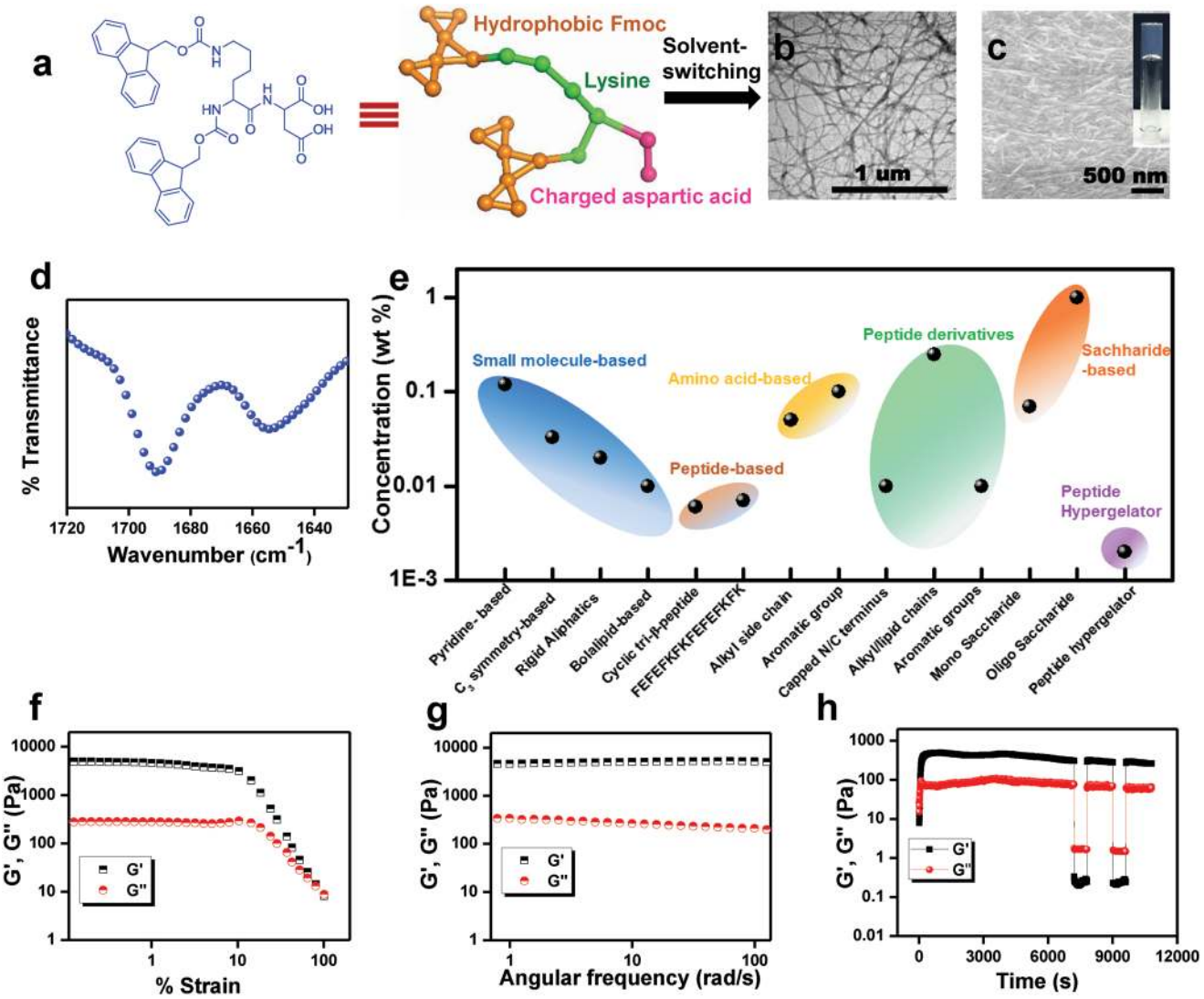

Figure 1. The Fmoc-Lys(Fmoc)-Asp hypergelator forms self-assembled hydrogel at a very low concentration. a) Chemical structure of Fmoc-Lys(Fmoc)-Asp containing hydrophobic Fmoc groups, lysine connector, and charged aspartic acid residue. b,c) TEM and HRSEM images of Fmoc-Lys(Fmoc)-Asp hydrogels. d) FTIR spectra of the dried hydrogels showing the amide I region. e) Comparison of the critical gelation concentration of different classes of hydrogelators including the present work. f) Strain sweep analysis of a 0.5 wt% hydrogel at a constant frequency of 1 Hz. g) Frequency-dependent oscillatory rheology of a 0.5 wt% hydrogel at 0.1% strain (within the LVR). h) Continuous step strain measurement at alternate 0.1% and 200% strain over time carried out on a 0.1 wt% hydrogel.

of 0.01 wt%.[27] Nevertheless, endeavors are continuing to identify smaller and simpler building blocks as hydrogelators with optimized CGC values.

Herein, we designed a minimalistic dipeptide-based hydrogelator, Fmoc-Lys(Fmoc)-Asp (Fmoc = 9-fluorenylmethyloxycarbonyl, Lys = lysine, Asp = aspartic acid, **Figure 1**a), which presented lowest CGC ever reported, 0.002 wt% (28.3×10^{-6} M), thus designating it a "hypergelator." The hypergelator, Fmoc-Lys(Fmoc)-Asp exhibited an unusual, hitherto unprecedented two-step self-assembly process. The functionality of the hydrogel was demonstrated in 3D cell culture as well as in composite material fabrication, where a conductive polymer was combined to yield a soft composite with ohmic conductivity. The soft conductive composite could also bind DNA, suggesting its potential application in DNA biochip fabrication.

Fmoc-protected amino acids or peptides have emerged as excellent building blocks for the development of functional self-assembled structures.[28] While most such building blocks include a single N-terminal protecting Fmoc group, our designed Fmoc-Lys(Fmoc)-Asp dipeptide includes an additional Fmoc group, protecting the Lys side chain (Figure 1a). Thus, modulation of the self-assembly process could potentially be obtained via additional H-bonding from the carbonyl group, aromatic and hydrophobic interactions from the fluorenyl ring, and steric optimization from the methoxycarbonyl moiety. The two hydrophilic carboxylic acid moieties at the C-terminus and the Asp side chain compensate for the hydrophobicity arising from the additional Fmoc group, thereby maintaining the balance between hydrophobic and hydrophilic functionalities necessary for self-assembly. The two carboxylic

acid groups provide not only potential noncovalent functionalization to the peptide, but also adequate doping capability of conductive polymer chains (vide infra), thus increasing its functionality.

Self-assembly and gelation of the Fmoc-Lys(Fmoc)-Asp dipeptide was carried out using the solvent-switch method.[21] Transmission electron microscopy (TEM) and high-resolution scanning electron microscopy (HRSEM) revealed the presence of entangled fibers following gelation, a characteristic of supramolecular hydrogels (Figure 1b,c). Fourier transform infrared spectroscopy (FTIR) analysis of the dried hydrogels (Figure 1d) exhibited two peaks at 1654 and 1691 cm^{-1} ascribed to the imperfect stacking of amide groups and stacked carbamate group of the Fmoc moiety, respectively.[29,30] Rheological studies were conducted to evaluate the mechanical properties of the hydrogel.[31] We investigated the time-dependent evolution of the storage and loss moduli (G' and G'', respectively) at different concentrations of the peptide (Figure S1, Supporting Information). The G' value was found to be higher than G'' at a concentration as low as 0.002 wt%, indicating the formation of a hydrogel. At a lower concentration (0.001 wt%), a hydrogel was not formed ($G' < G''$). Therefore, the CGC of the Fmoc-Lys(Fmoc)-Asp dipeptide is assessed to be 0.002 wt%, considerably lower than the lowest reported CGC, thus designating it a hypergelator.[18] Indeed, a comparison of the CGC values of different peptide and nonpeptide hydrogelators (Figure 1e, Table S1, Supporting Information) clearly indicates the superior gelation propensity of our designed protected dipeptide. Another intriguing observation arising from the time sweep curves (Figure S1, Supporting Information) is the manifestation of a two-step self-assembly process (at a concentration of 0.1 wt% and higher) which is unusual and, to our knowledge, unprecedented. Moreover, the fact that this characteristic is only observed at a concentration of 0.1 wt% and higher indicates that the two-step assembly is concentration-dependent.

Strain sweep experiments (Figure 1f) demonstrated a wide linear viscoelastic regime (LVR) and a breakage strain at 101%. Frequency sweep experiments (Figure 1g) revealed the independency of the modulus values with frequency along with higher values of G' over G'', confirming the gel nature. Finally, we observed the thixotropic property of the hydrogel as assessed by step strain experiments (Figure 1h). Circular dichroism (CD) spectra of the hydrogels (Figure S2, Supporting Information) indicated the absence of specific secondary structures of the peptide hypergelator, although the presence of a peak at 307 nm suggested strong π-stacking interactions.

In order to investigate the unusual two-step gelation (as shown in **Figure 2**a) in terms of the underlying supramolecular process, a combination of spectroscopic and microscopic techniques was employed. Time-dependent TEM images (Figure 2b) exhibited a morphological transformation from spheres to fibers over time suggesting a molecular rearrangement of the hypergelator, as observed for another Fmoc-protected gelator.[32] Powder X-ray diffraction (PXRD) performed on lyophilized hydrogels that were frozen at similar time-points (Figure 2c) showed the emergence of specific, nonsharp peaks over time, indicating the formation of long-range order in the self-assembled structures. Time-dependent UV–vis spectra of the hydrogel (Figure S3a, Supporting Information) exhibited peaks at 231, 283, and 305 nm which gradually blueshifted over time, indicating gelation by aggregation of the Fmoc groups. Interestingly, the 231 nm peak decreased in absorbance intensity, whereas the 283 nm peak increased. Fluorescence spectra of the hydrogels (Figure 2d) also exhibited a blue shift with a concomitant decrease in fluorescence intensity of the emission maxima over time, further indicating the aggregation of the Fmoc groups. Time-lapse photography of the hydrogel bulk formation (Figure 2e) revealed gelation after ≈15 min, already at the turbid state of the preparation, which correlates with the first increase step of the time-dependent rheology curve shown in Figure 2a. The apparent turbidity began to decrease after ≈45 min, corresponding to the second increase step of the time-dependent rheology curve (Figure 2a). The change in turbidity over time was also exhibited by a decrease of the OD values (Figure S3b, Supporting Information). Summarizing all these results, we hypothesize the two-step assembly to correlate with the morphological transition caused by supramolecular rearrangement of the hypergelator. The initial increase in G' and G'' (step 1) may be associated with the formation of spherical aggregates leading to the observed turbidity (t = 0 min) (Figure 2b,e). At t = 15 min, short fibers were observed along with the spherical aggregates (Figure 2b). These short fibers account for the gelation of the preparation in spite of the turbidity, an unusual process as the disappearance of turbidity is often correlated with gelation.[33] At t = 1 h, the spheres start dissolving into the fibers (Figure 2b) which leads to the second increment in the G' and G'' values (step 2, Figure 2a). The fact that only fibers were observed at 2.5 h (Figure 2b) designates the completion of the gelation process, as further demonstrated from the steady G' and G'' values over time (Figure 2a). Spectroscopic data support the formation of ordered assemblies by stacking of the Fmoc groups over time, associated with the supramolecular rearrangement process. We also performed TEM analysis on an ≈3 month aged Fmoc-Lys(Fmoc)-Asp gel in order to identify any phase transitions after the completion of fibrous structure formation. The fact that only fibers were observed in the TEM image (Figure S4, Supporting Information) indicates that there was no further phase transition after the nanofibrous structure had been reached.

To elucidate the molecular mechanism underlying the self-assembly process, solid-state NMR spectroscopy was employed. The hydrogel samples were frozen after 10 min, 1 h, or 2.5 h incubation, then lyophilized and subsequently assayed using ^{13}C CPMAS (cross-polarization under magic angle spinning) NMR. The NMR spectra of all three powder samples (Figure 2f) showed higher peak intensities for the carbons in the aromatic groups than those of the aliphatic groups. A possible explanation for this observation is that the transfer of magnetization from protons to ^{13}C nuclei is more efficient for the aromatic carbons, and/or that the conformation and surrounding environments are more ordered for the aromatic groups, thus rendering narrow spectral lines in the ^{13}C CPMAS NMR spectra. Comparing the spectra of samples with different incubation times, a downfield shift for all ^{13}C peaks from all aromatic and carbonyl groups occurred between the 1 and 2.5 h incubation, possibly corresponding to the second morphological transition observed in the time-dependent TEM images (step 2 of

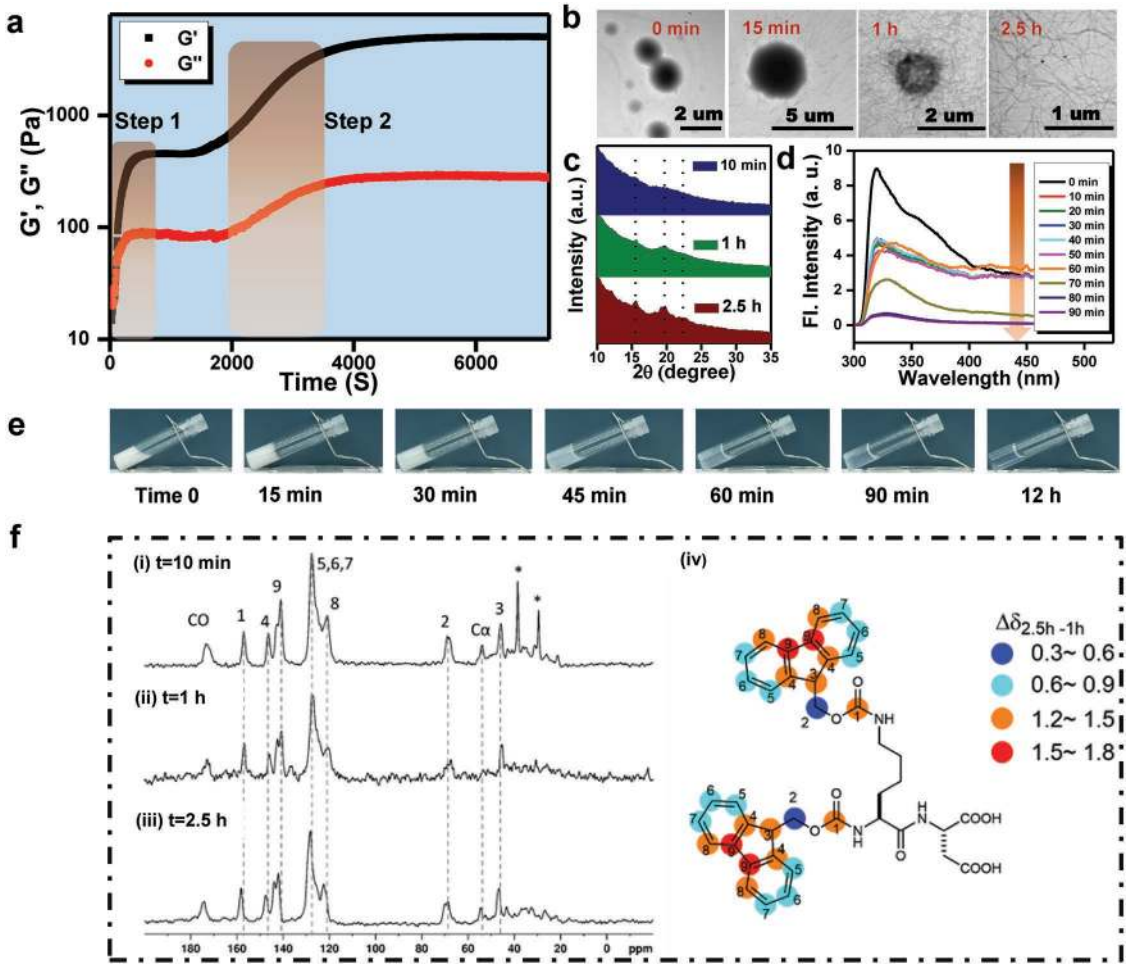

Figure 2. Two-step assembly process of the Fmoc-Lys(Fmoc)-Asp hydrogel. a) Time-dependent evolution of *G′* and *G″* exhibiting a two-step growth of a 0.5 wt% hydrogel. b) TEM images of Fmoc-Lys(Fmoc)-Asp hydrogel at different time points. c) Powder X-ray diffraction patterns of lyophilized hydrogels frozen at different time points. d) Fluorescence emission spectra of the hydrogels (0.1 wt%) at different time points. e) Optical images at different time points exhibiting the decreasing turbidity during the gelation of a 0.5 wt% preparation. f) Carbon-13 CPMAS NMR spectra of lyophilized Fmoc-Lys(Fmoc)-Asp hydrogel samples (0.5 wt%) frozen at different time points. i–iii) ^{13}C CPMAS NMR spectra of lyophilized Fmoc-Lys(Fmoc)-Asp hydrogel frozen after 10 min (i), 1 h (ii), 2.5 h (iii) of incubation. Spectra were recorded under 15 kHz MAS condition. Downfield shift of aromatic signals by ≈1 to 2 ppm was observed after 2.5 h incubation. Asterisks indicate the peaks of adamantane as an internal reference for ^{13}C chemical shift. iv) Chemical structure of Fmoc-Lys(Fmoc)-Asp with numbering of carbon atoms in Fmoc groups.

the time-dependent rheology curve, Figure 2a). Several reports using quantum chemical calculations have suggested that ^{13}C NMR peaks of aromatic carbons shift to downfield because of the aromatic ring stacking.[34–38] In addition, experimental results obtained from several compounds have demonstrated that the molecular packing in crystal and aggregated structures causes downfield shift of molecules.[39,40] Comparing the downfield shifts of the 1 and 2.5 h samples, chemical shifts for the center region of aromatic rings (C4, C8, C9) shift larger compared to other groups and that of the carbons outside aromatic rings (C2). This may imply that chemical shifts of aromatic groups were influenced by both molecular packing and π-stacking, while that of C2 was affected only by molecular packing. In addition, the chemical shift of the Cα carbons did not shift significantly when compared to aromatic carbons, although this signal could not be observed for the 1 h samples. Although the chemical shift of carbamate carbon shifted larger than that of the C2, C3, C5, C6, C7 carbons, the chemical shifts of the carbonyl groups are easily influenced by hydrogen bonding. Thus, it is possible that the carbamate carbon takes part in the formation of hydrogen bonding. Based on these NMR experiments, it can be surmised that π-stacking and molecular packing increase over time, thereby playing a crucial role in the second step of the gelation process.

Molecular dynamics is one simulation approach commonly utilized to investigate the self-assembly behavior of peptides and peptide derivatives.[41–43] To further explore the self-assembly mechanism, we performed three microsecond coarse-grained molecular dynamics (CG-MD) simulations on systems consisting of 400 Fmoc-Lys(Fmoc)-Asp molecules in aqueous solutions containing ≈10% dimethyl sulfoxide (DMSO) in volume. Simulation details are given in the Supporting Information. The peptide concentration was 30 mg mL^{-1}. Simulations at low peptide concentrations, as experimentally used, are computationally

intensive. In order to reduce the need of computational power and accelerate the assmebly process, we set the peptide concentrations in our simulations to be much higher, in accordence with previous simulation studies.[30,43–45] Each Fmoc-Lys(Fmoc)-Asp molecule was modeled by 14 hydrophobic beads for the Fmoc groups, two negatively charged beads for the Asp group, and five beads for the Lys group (lysine is neutral). The three groups are colored in orange, red, and green, respectively (**Figure 3**a). Interaction type of each bead is shown in Figure S5 (Supporting Information).

As shown in Figure 3b–h, 400 randomly dispersed Fmoc-Lys(Fmoc)-Asp molecules aggregate quickly and form ordered oligomers (such as dimers and trimers), which are stabilized by the parallel stacking of Fmoc fluorene rings (see the snapshot at 0.02 μs). These oligomers grow into thin fibers by monomer or oligomer addition (see the snapshot at 0.1 μs). Some of the fibers consist of a well-aligned single layer of fluorene rings (with a thickness of ≈0.7 nm), while others consist of two layers of fluorene rings (with a thickness of ≈1.5 nm). Then, the single-layer fibers fuse into double-layer ones, and at the same time the double-layer fibers grow longer along the fibril axis. At 0.5 μs, almost all of the fibers comprise double layers of fluorene rings. After 1.0 μs, short branches start to form along the directions almost perpendicular to the fibril axis. Meanwhile, the fibrils grow, bend, and form branched fibrils. Finally, a delicate branched fibril forms at 6.0 μs, reminiscent of a hydrogel. Surprisingly, all the fibril filaments have a uniform thickness of ≈1.5 nm (comprising a double layer of fluorene rings).

To investigate the different roles of the Fmoc, Asp, and Lys groups in the self-assembly process, we calculated the fraction of their solvent accessible surface area (SASA). As shown in Figure 3i, the SASA fraction of the Fmoc group drops rapidly within the first 1 μs, then continues to decrease slowly and reaches a value of 0.16 at $t = 5$ μs, whereas the SASA fraction of Lys gradually decreases to 0.25. In sharp contrast, the SASA fraction of Asp quickly increases and reaches a plateau of 0.58 after $t = 5$ μs. We further calculated the contact number between each pair of groups in order to reveal the interactions crucial for hydrogel formation. As shown in Figure 3j, the Fmoc-Fmoc group pair has the highest contact number, 2.684, indicating the strongest interaction between Fmoc groups. The contact number between Fmoc groups and Lys groups is ranked second, with an average contact number of 2.107. Other group pairs have much smaller contact numbers, especially the Asp-Asp group pair, with a contact number of only 0.021. This small contact number is attributed to the strong electrostatic repulsion between two Asp groups. These data indicate that the Fmoc groups strongly interact with each other and with the Lys groups. These two groups have a preference to be buried inside the hydrogel and form the fibril hydrophobic core, while the Asp groups have a strong tendency to be solvent-exposed (Figure 3k).

In order to reveal the formation mechanism of the fibril hydrophobic core, we further examined the aromatic stacking patterns of the Fmoc groups in the hypergelator assemblies by calculating the free energy landscape as a function of the centroid distance and the angle between two aromatic rings. As there are two Fmoc groups in each Fmoc-Lys(Fmoc)-Asp molecule, we calculated the free energy landscape separately for inter- and intramolecular Fmoc group pairs. In the free energy surface of intramolecular Fmoc groups, one deep minimum-energy basin is located at a (angle, centroid distance) value of (10°, 0.45 nm), indicating a strong preference of parallel stacking (Figure 3l). However, two minimum energy basins are observed in the free energy surface of intermolecular Fmoc groups. These are located at (10°, 0.45 nm) and (80°, 0.45 nm), implying that in addition to the parallel stacking patterns, perpendicular (i.e., T-shaped) stacking patterns are also preferred (Figure 3m). These data indicate that the hydrophobic core of the fibril is formed by Fmoc groups through both inter- and intramolecular π-stackings. As shown in Figure 3n, the T-shaped stacking pattern is located at the intersection point of two fibril branches, revealing its importance to the formation of hydrogels.

As mentioned above, at a peptide concentration of 30 mg mL^{-1}, Fmoc-Lys(Fmoc)-Asp molecules form hydrogels with a uniform fibril thickness of ≈1.5 nm. To elucidate the two-step self-assembly of the hydrogel from a molecular point of view, we performed six additional 6 μs MD simulations at two elevated peptide concentrations (59 and 100 mg mL^{-1}). The final snapshots of all nine simulations (at concentrations of 30, 59, and 100 mg mL^{-1}) are shown in **Figure 4**a–c and Figure S6 (Supporting Information). Surprisingly, hydrogels formed at elevated concentrations also consist of multiple intercrossed fibrils with a thickness of ≈1.5 nm, similar to the hydrogel formed at 30 mg mL^{-1}. However, hydrogels formed at 59 and 100 mg mL^{-1} display many more branches than formed at 30 mg mL^{-1} (Figure 4d–f). The increase of fibril branches can also be reflected and understood from the free energy landscape shown in Figure 4g–i. The free energy landscape at each concentration exhibits two minimum energy basins at (10°, 0.45 nm) and (80°, 0.45 nm), corresponding to parallel and T-shaped stacking patterns of Fmoc fluorene rings, respectively. The parallel-stacking energy basins are much deeper than the T-shaped ones, indicating that fibril growth along the fibril axis is more energy-favorable than fibril branching. Interestingly, with the increase of peptide concentration, the parallel-stacking basin does not change much, while the T-shaped-stacking basin becomes deeper. These results indicate a competition between fibril growth and fibril branching. At the low concentration (30 mg mL^{-1}), fibril growth along one dimension is dominant, leading to the prolate-shaped hydrogel-like aggregates (yellow circle in Figure 4j). At the medium concentration (59 mg mL^{-1}), the competitiveness of branching is enhanced. The fibrils grow along two dimensions and form oblate-shaped hydrogel-like aggregates (red circle in Figure 4j). At the highest concentration (100 mg mL^{-1}), fibril branching becomes more competitive, which allows the fibrils to grow along three dimensions, and sphere-like hydrogel aggregates are formed (blue circle in Figure 4j). Recently, by performing MD simulations in combination with MARTINI force field, Huang and co-workers investigated the self-assembly mechanisms of PYR nanotube and PYN nanovesicle.[45] Their simulations demonstrated that the two largely similar amphiphiles PYR and PYN preferred distinct assembly pathways, which can lead to drastically different self-assembled structures, implying the self-assembly of PYR nanotube and PYN nanovesicle is kinetically controlled. To further explore the self-assembly mechanism of the Fmoc-Lys(Fmoc)-Asp hydrogel, we calculated the time evolution of the largest

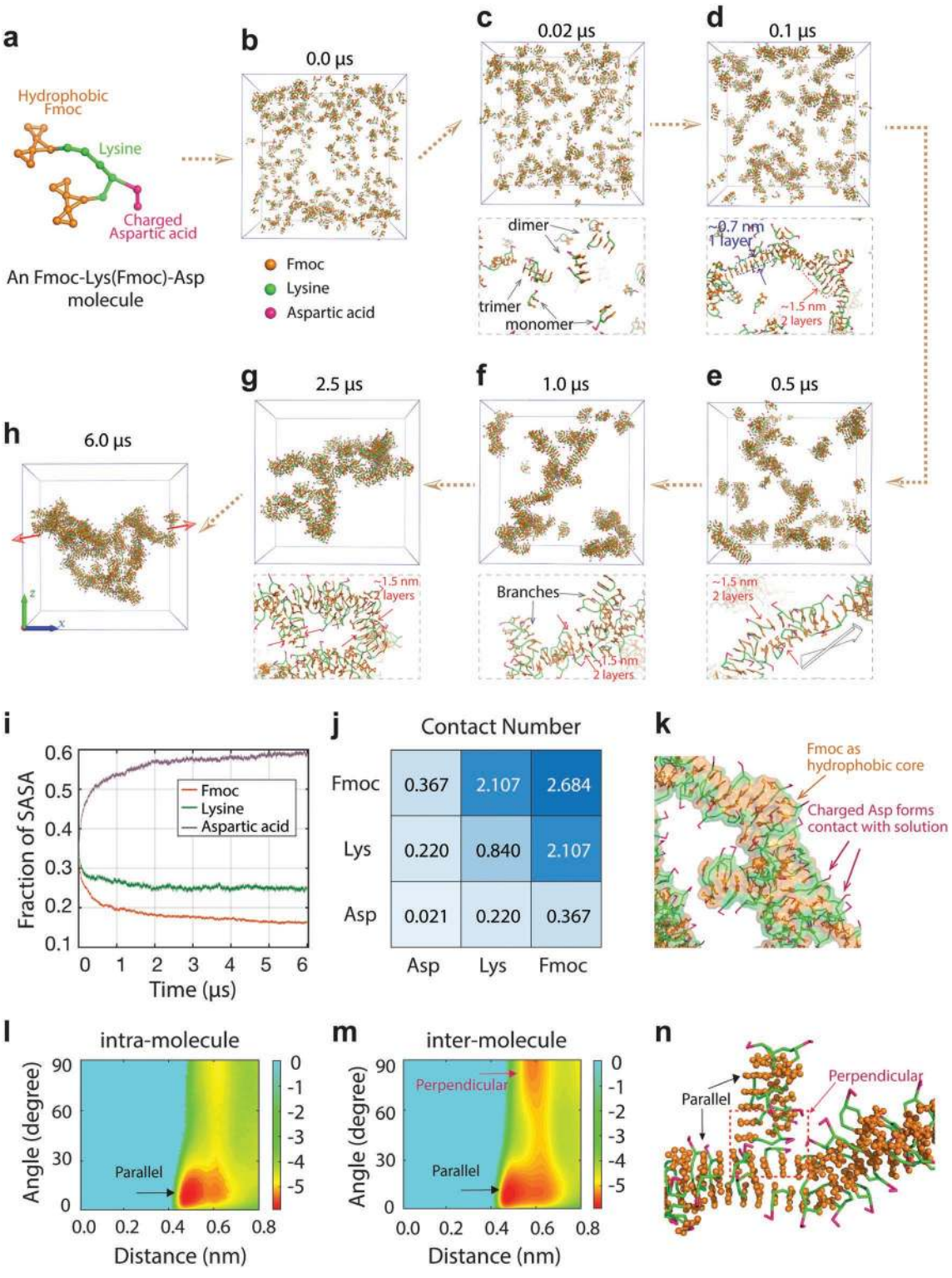

Figure 3. Self-assembly pathway and mechanism of Fmoc-Lys(Fmoc)-Asp hydrogel probed by microsecond-long CG-MD simulations. a) Coarse-grained model of an Fmoc-Lys(Fmoc)-Asp molecule. b–h) Snapshots of Fmoc-Lys(Fmoc)-Asp aggregates at seven different time points, showing the self-assembly pathway. Detailed local structures are also shown for the five intermediate time points. i) Time evolution of the SASA fraction of the Fmoc, lysine, and aspartic acid groups. j) Average contact number for different group pairs calculated using the last 1 μs data of simulation. k) Illustration of the self-assembly mechanism of Fmoc-Lys(Fmoc)-Asp hydrogels. The hydrophobic core formed by Fmoc and Lys is shown in surface representations while the solution-exposed Asp residues are shown as purple sticks. l,m) The free energy landscapes of the intra- and intermolecular Fmoc stackings plotted as a function of the centroid distance and the angle between two aromatic rings. n) The parallel and T-shaped stacking patterns.

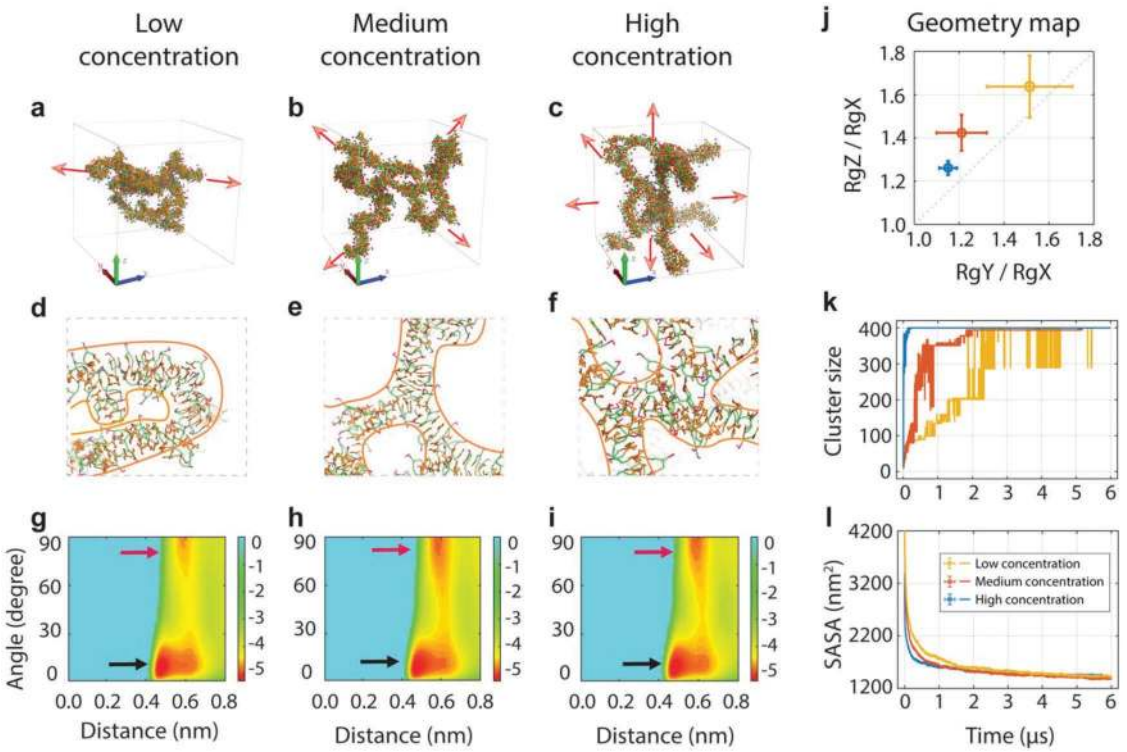

Figure 4. Analyses of structures and self-assembly pathways of Fmoc-Lys(Fmoc)-Asp hydrogels at different peptide concentrations. a–c) Snapshots of Fmoc-Lys(Fmoc)-Asp hydrogels. d–f) Detailed local structures of Fmoc-Lys(Fmoc)-Asp hydrogels. g–i) The free energy landscapes of the intermolecular Fmoc stacking plotted as a function of the centroid distance and the angle between two aromatic rings. j) Geometry map of the Fmoc-Lys(Fmoc)-Asp hydrogels formed. The dotted line indicates the diagonal of the map. k,l) Time evolution of the size of the largest cluster and the SASA of the aggregates.

cluster size and the SASA at each Fmoc-Lys(Fmoc)-Asp concentration. At the highest concentration (blue line in Figure 4k), the size of the largest cluster increases rapidly and reaches its maximum value of 400 in less than 200 ns, corresponding to the formation of one single aggregate. At lower concentrations, the increase of the largest cluster size is much slower, accompanying the fusion of small clusters into larger aggregates (red and yellow lines in Figure 4k), and the largest cluster size reaches 400 within 2.5 μs. However, the SASA values at all concentrations still gradually decrease after the formation of one single aggregate (Figure 4l). The gradual decrease of SASA values is accompanied by the structural relaxation towards thermodynamically stable gel-like aggregates. These results indicate that the self-assembly of the Fmoc-Lys(Fmoc)-Asp hydrogel mostly progresses through thermodynamic control.

These results provide explanations for the experimentally observed two-step growth process. The hydrogel formation process is accompanied by the dissolution of the preformed peptide plaques. As shown in the TEM image (Figure 2b), at 15 min the plaque is ≈3.5 μm in diameter. This plaque then gradually dissolves and becomes smaller with a diameter of ≈1.3 μm at the 1 h time point. At 2.5 h, thin and branched fibrils are formed, and the plaque totally dissolves into the aqueous solution. The dissolution of plaques may increase local peptide concentration, resulting in stepwise self-assembly process. This analysis is also in agreement with the observation that the two-step assembly was observed only at higher experimental concentrations (above a concentration of 0.1 wt%) of the hypergelator (Figure S1, Supporting Information). Therefore, the two-step assembly is explained in terms of underlying supramolecular as well as molecular processes, though the relative contribution of each factor is yet unknown.

In order to assess the uniqueness of our molecular design in terms of gelation efficiency, as well as relate the two-step assembly to a specific moiety in the peptide, we studied the self-assembly of several peptide analogues. These included dipeptides of identical sequence but protected only by a single Fmoc group, namely, NH_2-Lys-(Fmoc)-Asp and Fmoc-Lys-Asp, as well as dipeptides in which Asp was substituted with nonpolar (Ala, Cys, Pro, Leu, Phe), polar (Asn, Tyr, Ser), or positively charged (Arg, His) amino acids. The results of the self-assembly study of these peptides are summarized in **Table 1**. Apart from Fmoc-Lys-Asp and Fmoc-Lys(Fmoc)-Tyr, all peptides proved aggregative and in most cases formed ordered nanostructures. Importantly, Fmoc-Lys(Fmoc)-Ala, Fmoc-Lys(Fmoc)-Cys, Fmoc-Lys(Fmoc)-Asn, and Fmoc-Lys(Fmoc)-His formed hydrogels, but with lower mechanical strength and considerably higher CGC value compared to the originally designed hypergelator. Additional details of the self-assembly study of the analogues are provided in the Supporting Information (Figures S7–S13, Supporting Information). Interestingly, we observed the two-step self-assembly process in 0.5 wt% hydrogels of Fmoc-Lys(Fmoc)-Ala. The self-assembly studies of this library of peptides thus attest to the superiority of the hypergelator in terms of gelation efficiency. The fact that the two-step growth was only observed for Fmoc-Lys(Fmoc)-Ala amongst all other peptide analogues

Table 1. Characteristics of the studied peptide analogues. The originally designed peptide, Fmoc-Lys(Fmoc)-Asp, is shown for comparison. For detailed characterization of the peptide analogues see Figures S7–S13 (Supporting Information).

Peptides studied	Aggregation behavior	Morphology		*G′* value of 0.5 wt% gel [Pa]	CGC [wt%]
NH_2-Lys(Fmoc)-Asp	Very weak hydrogel		Fiber	–	–
Fmoc-Lys-Asp	No aggregation			–	–
Fmoc-Lys(Fmoc)-Asp	Hydrogel		Fiber	5031	0.002
Fmoc-Lys(Fmoc)-Ala	Hydrogel		Fiber	1653	>0.05
Fmoc-Lys(Fmoc)-Cys	Weak hydrogel	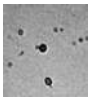	Fiber +vesicle	286	>0.05
Fmoc-Lys(Fmoc)-Asn	Hydrogel		Fiber	4048	>0.05
Fmoc-Lys(Fmoc)-His	Hydrogel		Fiber	640	>0.05
Fmoc-Lys(Fmoc)-Pro	No gelation (turbid solution + precipitates)		Vesicle	–	–
Frnoc-Lys(Fmoc)-Leu	No gelation (turbid solution + precipitates)		Joint vesicle	–	–
Finoc-Lys(Fmoc)-Phe	Inhoinogeneous hydrogel		Fiber	–	–
Fmoc-Lys(Fmoc)-Ser	Inhomogeneous hydrogel		Fiber	–	–
Fmoc Lys(Fmoc) Tyr	Precipitate		Irregular aggregates	–	–
Fmoc-Lys(Fmoc)-Arg	Precipitate at the bottom + assembly		Fiber	–	–

suggests that the relation between the process and the molecular structure of the gelators is not straightforward. However, both Fmoc-Lys(Fmoc)-Ala and Fmoc-Lys(Fmoc)-Asp have C-terminal residues with simpler structures compared to the other analogues. This possibly underlies the identical self-assembly patterns of the two peptides leading to the two-step growth process.

Finally, we demonstrated the functional properties of the designed hydrogelator. In order to evaluate the usability of the hydrogel as a soft 2D/3D cell scaffold, its cytotoxicity was tested.

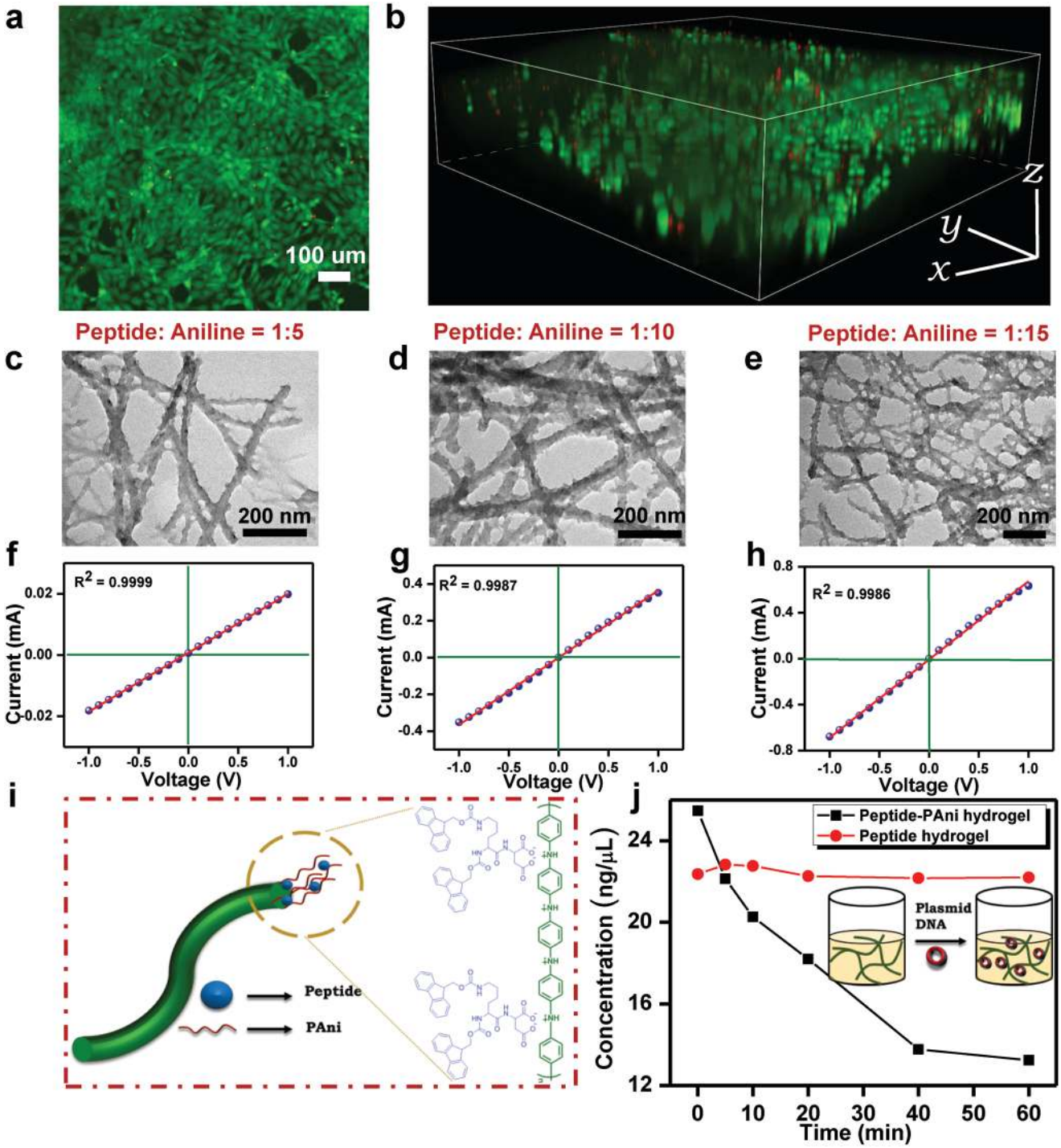

Figure 5. Functional properties of the Fmoc-Lys(Fmoc)-Asp hydrogel and its conductive composite. a) Live/dead staining of 3T3 fibroblast cells cultured on the 0.5 wt% hydrogel surface (2D cell culture). Green staining indicates live cells; red staining indicates dead cells. b) 3D volume rendering images obtained by Z-stack of confocal microscopy images showing 3T3 fibroblast cells in a 0.5 wt% hydrogel ($x = y = 1272.79$ μm, $z = 363.44$ μm). c–e) TEM images of composite hydrogels prepared by in situ polymerization of aniline inside Fmoc-Lys(Fmoc)-Asp hydrogels (0.5 wt%) at different molar ratios of peptide and aniline. f–h) *I–V* characteristics of the dried composite hydrogels at peptide:aniline molar ratios of 1:5, 1:10, and 1:15. i) Illustration of the probable structure of the composite fibers. j) DNA binding by the composite peptide–PAni hydrogel.

2,3-Bis(2-methoxy-4-nitro-5-sulfophenyl)-2H-tetrazolium-5-carboxanilide (XTT) analysis (Figure S14, Supporting Information) indicated the hydrogel to be highly cytocompatible.[46] Next, fibroblasts were seeded on top of the hydrogels and tested by Live/Dead staining in situ. A large population of spindle-shaped green cells were observed after 1 d (**Figure 5**a),

indicating the facilitation of cell adherence by the hydrogel. Moreover, 4 d following seeding, migration of the cells into the hydrogel bulk was observed using confocal scanning laser microscopy (Figure 5b). The migration depth was found to be ≈363 µm, a value higher than those reported for other supramolecular hydrogels.[22,47] Therefore, the hydrogel clearly exhibits potential as a 3D cell scaffolding material.

The range of applications of the hypergelator-based hydrogel can be further expanded by utilizing it for producing a conductive soft composite. Conductive soft materials/gels have emerged as an exciting class of materials with diverse applications ranging from biotechnology to electronics.[48,49] Composite hydrogels composed of short peptides and conductive polymers are especially interesting as they harness the intrinsic biocompatibility and mechanical property of peptide hydrogels with the conductivity of the conductive polymers.[50] Here, we anticipated that the two carboxylic acid groups of the C-terminal Asp would be sufficient to dope the conductive polymers. We prepared conductive hydrogels composed of the hypergelator and polyaniline (PAni) by oxidative polymerization of aniline in situ[50] at three different molar ratios of peptide and aniline. TEM images of the composite hydrogels showed fibers with a rugged surface (Figure 5c–e), resembling a previously reported peptide–PAni composite hydrogel.[50] UV–vis characterization of the composite PAni hydrogels (Figure S15, Supporting Information) exhibited typical peaks for PAni, indicating it to be in a sufficiently doped, conductive, emeraldine salt form.[51] Current–voltage (*I*–*V*) characteristics of the dried composite hydrogels exhibited an ohmic response (Figure 5f–h), indicating their metallic-like characteristics.[50] A cartoon representation (Figure 5i) provides a probable explanation of the peptide–PAni fiber formation, by which the hydrophilic Asp residues remaining on the outer surface of the fibers adequately dope the PAni chains, thus generating polarons[50] that result in the highly conductive emeraldine salt form.

DNA biochips have gained significant attention due to their rapid and effective detection of pathogens by presenting DNA sequences that are covalently bound to a solid substrate. Yet, 2D DNA chips remain limited by their hybridization efficacy, as well as the loading capacity of the surface materials. Our 3D peptide–PAni composite hydrogels present positive charges on their fiber surface owing to the positively charged PAni chains, and therefore have potential for DNA binding. The high water content and 3D structure of the hydrogel composites may increase the DNA loading capacity and allow its utilization as efficient DNA immobilizing material. We evaluated the DNA binding ability of the peptide–PAni composite-hydrogels using an absorbance-based assay (Figure 5j). Evidently, the concentration of the DNA decreased significantly over time for the peptide–PAni composite indicating its binding, whereas the peptide-only hydrogel failed to show any ability to bind DNA. The electrostatic attraction between the positively charged peptide–PAni fibers and the negatively charged plasmid DNA underlies the DNA binding feature of the peptide–PAni composite material. This result highlights the potential of the peptide–PAni composite hydrogel as a component for engineering 3D DNA biochips.

In summary, we designed a double Fmoc group-containing hypergelator which self-assembles to form a hydrogel at an extremely low concentration. The hypergelator exhibits an unusual two-step assembly process. Self-assembly studies of several analogues of the gelator attest to the specificity of the molecular structure required for obtaining a very low CGC. Generally, the studied library of di-Fmoc-based dipeptides suggests that these building blocks could act as efficient peptide hydrogelators. From the applicative perspective, the hydrogel is suitable for 2D/3D cell scaffolding and for the preparation of conductive composite hydrogels based on conducting polymer incorporation. The peptide–PAni composite hydrogel was successfully utilized for DNA binding. Therefore, this dipeptide-based hydrogel is a very interesting soft material in terms of design, properties and applications.

Supporting Information

Supporting Information is available from the Wiley Online Library or from the author.

Acknowledgements

G.W. acknowledges the financial support from National Key Research and Development Program of China (2016YFA0501702) and the National Science Foundation of China (Grant No. 11674065). This work was partially supported by grants from the European Research Council under the European Union's Horizon 2020 research and innovation program (BISON, Advanced ERC Grant No. 694426) (E.G.). T.Y. was supported by Uehara Memorial Foundation. T.G. acknowledges support from the Argentinean Friends of Tel Aviv University. P.C. gratefully acknowledges the Center for Nanoscience and Nanotechnology of Tel Aviv University for financial support and thanks the members of the Gazit laboratory for helpful discussions. 3T3 mouse fibroblast cells used in this study were purchased from ATCC.

Conflict of Interest

The authors declare no conflict of interest.

Keywords

conductive composites, dipeptide, molecular dynamics, self-assembly, two-step gelation

Received: September 15, 2019
Revised: December 3, 2019
Published online: January 27, 2020

[1] G. M. Whitesides, B. Grzybowski, *Science* **2002**, *295*, 2418.
[2] S. Zhang, *Nat. Biotechnol.* **2003**, *21*, 1171.
[3] G. M. Whitesides, J. P. Mathias, C. T. Seto, *Science* **1991**, *254*, 1312.
[4] M. Reches, E. Gazit, *Science* **2003**, *300*, 625.
[5] P. F. Nealey, J. J. de Pablo, S. O. Kim, N. J. Ferrier, M. P. Stoykovich, H. H. Solak, *Nature* **2003**, *424*, 411.
[6] R. Nelson, M. R. Sawaya, M. Balbirnie, A. Madsen, C. Riekel, R. Grothe, D. Eisenberg, *Nature* **2005**, *435*, 773.
[7] C. M. Dobson, *Nature* **2003**, *426*, 884.

[8] P. C. Ke, M. A. Sani, F. Ding, A. Kakinen, I. Javed, F. Separovic, T. P. Davis, R. Mezzenga, *Chem. Soc. Rev.* **2017**, *46*, 6492.
[9] J. D. Hartgerink, E. Beniash, S. I. Stupp, *Science* **2001**, *294*, 1684.
[10] R. Mezzenga, P. Fischer, *Rep. Prog. Phys.* **2013**, *76*, 046601.
[11] S. Bera, S. Mondal, B. Xue, L. J. W. Shimon, Y. Cao, E. Gazit, *Nat. Mater.* **2019**, *18*, 503.
[12] L. Adler-Abramovich, D. Aronov, P. Beker, M. Yevnin, S. Stempler, L. Buzhansky, G. Rosenman, E. Gazit, *Nat. Nanotechnol.* **2009**, *4*, 849.
[13] T. P. J. Knowles, T. W. Oppenheim, A. K. Buell, D. Y. Chirgadze, M. E. Welland, *Nat. Nanotechnol.* **2010**, *5*, 204.
[14] S. Zhang, M. A. Greenfield, A. Mata, L. C. Palmer, R. Bitton, J. R. Mantei, C. Aparicio, M. O. De La Cruz, S. I. Stupp, *Nat. Mater.* **2010**, *9*, 594.
[15] K. Tao, P. Makam, R. Aizen, E. Gazit, *Science* **2017**, *358*, eaam9756.
[16] X. Yan, P. Zhu, J. Li, *Chem. Soc. Rev.* **2010**, *39*, 1877.
[17] L. A. Estroff, A. D. Hamilton, *Chem. Rev.* **2004**, *104*, 1201.
[18] X. Du, J. Zhou, J. Shi, B. Xu, *Chem. Rev.* **2015**, *115*, 13165.
[19] S. Fleming, R. V. Ulijn, *Chem. Soc. Rev.* **2014**, *43*, 8150.
[20] D. J. Adams, *Macromol. Biosci.* **2011**, *11*, 160.
[21] A. Mahler, M. Reches, M. Rechter, S. Cohen, E. Gazit, *Adv. Mater.* **2006**, *18*, 1365.
[22] X. Q. Dou, C. L. Feng, *Adv. Mater.* **2017**, *29*, 1604062.
[23] E. F. Banwell, E. S. Abelardo, D. J. Adams, M. A. Birchall, A. Corrigan, A. M. Donald, M. Kirkland, L. C. Serpell, M. F. Butler, D. N. Woolfson, *Nat. Mater.* **2009**, *8*, 596.
[24] S. Zhang, X. Zhao, L. Spirio, *Encyclopedia of Biomedical Polymers and Polymeric Biomaterials*, Taylor and Francis, London, UK **2016**, pp. 6894–6908.
[25] H. Misawa, A. Yoshida, M. Tanaka, H. Endo, T. Ozaki, N. Kobayashi, A. Soto-Gutierrez, Y. Chen, J. D. Rivas-Carrillo, N. Navarro-Alvarez, K. Tanaka, A. Miki, N. Tanaka, J. Takei, T. Ueda, *Cell Transplant.* **2006**, *15*, 903.
[26] K. Wang, J. D. Keasling, S. J. Muller, *Int. J. Biol. Macromol.* **2005**, *36*, 232.
[27] Y. Tian, H. Wang, Y. Liu, L. Mao, W. Chen, Z. Zhu, W. Liu, W. Zheng, Y. Zhao, D. Kong, Z. Yang, W. Zhang, Y. Shao, X. Jiang, *Nano Lett.* **2014**, *14*, 1439.
[28] K. Tao, A. Levin, L. Adler-Abramovich, E. Gazit, *Chem. Soc. Rev.* **2016**, *45*, 3935.
[29] S. Fleming, P. W. J. M. Frederix, I. Ramos Sasselli, N. T. Hunt, R. V. Ulijn, T. Tuttle, *Langmuir* **2013**, *29*, 9510.
[30] P. W. J. M. Frederix, G. G. Scott, Y. M. Abul-Haija, D. Kalafatovic, C. G. Pappas, N. Javid, N. T. Hunt, R. V. Ulijn, T. Tuttle, *Nat. Chem.* **2015**, *7*, 30.
[31] C. Yan, D. J. Pochan, *Chem. Soc. Rev.* **2010**, *39*, 3528.
[32] G. Fichman, T. Guterman, J. Damron, L. Adler-Abramovich, J. Schmidt, E. Kesselman, L. J. W. Shimon, A. Ramamoorthy, Y. Talmon, E. Gazit, *Sci. Adv.* **2016**, *2*, e1500827.
[33] R. Orbach, L. Adler-Abramovich, S. Zigerson, I. Mironi-Harpaz, D. Seliktar, E. Gazit, *Biomacromolecules* **2009**, *10*, 2646.
[34] D. Sundholm, M. Rauhalahti, N. Özcan, R. Mera-Adasme, J. Kussmann, A. Luenser, C. Ochsenfeld, *J. Chem. Theory Comput.* **2017**, *13*, 1952.
[35] J. Czernek, *J. Phys. Chem. A* **2003**, *107*, 3952.
[36] J. A. Platts, K. Gkionis, *Phys. Chem. Chem. Phys.* **2009**, *11*, 10331.
[37] J. Trykowska, E. Hejchman, I. Wolska, D. Maciejewska, *J. Mol. Struct.* **2009**, *930*, 195.
[38] S. Miyajima, T. Chiba, G. Saito, H. Inokuchi, *J. Phys. Chem.* **1995**, *99*, 1582.
[39] H. Kurosu, T. Ookubo, H. Tuchiya, I. Ando, J. Watanabe, *J. Mol. Struct.: Theochem* **2001**, *574*, 153.
[40] D. L. Vanderhart, *J. Magn. Reson.* **1981**, *44*, 117.
[41] C. Guo, Y. Luo, R. Zhou, G. Wei, *ACS Nano* **2012**, *6*, 3907.
[42] P. W. J. M. Frederix, R. V. Ulijn, N. T. Hunt, T. Tuttle, *J. Phys. Chem. Lett.* **2011**, *2*, 2380.
[43] V. Basavalingappa, T. Guterman, Y. Tang, S. Nir, J. Lei, P. Chakraborty, L. Schnaider, M. Reches, G. Wei, E. Gazit, *Adv. Sci.* **2019**, *6*, 1900218.
[44] N. Brown, J. Lei, C. Zhan, L. J. W. Shimon, L. Adler-Abramovich, G. Wei, E. Gazit, *ACS Nano* **2018**, *12*, 3253.
[45] X. Zheng, L. Zhu, X. Zeng, L. Meng, L. Zhang, D. Wang, X. Huang, *J. Phys. Chem. Lett.* **2017**, *8*, 1798.
[46] G. F. Liu, D. Zhang, C. L. Feng, *Angew. Chem., Int. Ed.* **2014**, *53*, 7789.
[47] P. Li, Z. Yin, X. Q. Dou, G. Zhou, C. L. Feng, *ACS Appl. Mater. Interfaces* **2014**, *6*, 7948.
[48] P. Chakraborty, S. Das, A. K. Nandi, *Prog. Polym. Sci.* **2019**, *88*, 189.
[49] B. W. Walker, R. P. Lara, E. Mogadam, C. Hsiang Yu, W. Kimball, N. Annabi, *Prog. Polym. Sci.* **2019**, *92*, 135.
[50] P. Chakraborty, T. Guterman, N. Adadi, M. Yadid, T. Brosh, L. Adler-Abramovich, T. Dvir, E. Gazit, *ACS Nano* **2019**, *13*, 163.
[51] J. Stejskal, P. Kratochvíl, N. Radhakrishnan, *Synth. Met.* **1993**, *61*, 225.